Gravitational-Wave Data Analysis with High-Precision Numerical Relativity Simulations of Boson Star Mergers

Tamara Evstafyeva,[1,*] Ulrich Sperhake,[1,2,3,†] Isobel M. Romero-Shaw,[1,4,‡] and Michalis Agathos[1,4,5,§]

[1]DAMTP, Centre for Mathematical Sciences, University of Cambridge, Wilberforce Road, Cambridge CB3 0WA, United Kingdom
[2]Department of Physics and Astronomy, Johns Hopkins University, 3400 North Charles Street, Baltimore, Maryland 21218, USA
[3]TAPIR 350-17, Caltech, 1200 E. California Boulevard, Pasadena, California 91125, USA
[4]Kavli Institute for Cosmology Cambridge, Madingley Road Cambridge CB3 0HA, United Kingdom
[5]School of Mathematical Sciences, Queen Mary University of London, Mile End Road, London, E1 4NS, UK

(Received 4 June 2024; accepted 23 July 2024; published 24 September 2024)

Gravitational-wave signals detected to date are commonly interpreted under the paradigm that they originate from pairs of black holes or neutron stars. Here, we explore the alternative scenario of boson-star signals being present in the data stream. We perform accurate and long (∼20 orbits) numerical simulations of boson-star binaries and inject the resulting strain into LIGO noise. Our Bayesian inference reveals that some boson-star signals are degenerate with current approximants, albeit with biased parameters, while others exhibit smoking-gun signatures leaving behind conspicuous residuals.

DOI: 10.1103/PhysRevLett.133.131401

Introduction—Following the Nobel-Prize winning detection of GW150914 [1], about 100 further gravitational-wave (GW) events have been confidently detected by the laser interferometer gravitational-wave observatory (LIGO) and Virgo [2–4]. This ever-increasing ensemble of GW events provides ample opportunities to explore some of the deepest mysteries of the cosmos and test the nature of compact objects: black holes (BHs), neutron stars (NSs) and exotic compact objects (ECOs) [5]. A research program targeting such tests, however, faces several crucial challenges: (i) Given a candidate class of ECOs, can we generate gravitational waveforms of sufficient longevity and accuracy? (ii) Supposing ECO coalescences occur in the Universe, can we detect them with our current search pipelines? (iii) If yes, can we distinguish them from traditional binary BH (BBH) or NS events? (iv) Can we generate comprehensive GW template banks suitable as alternatives to BH and NS approximants for parameter estimation (PE)? The main goal of this Letter is to explore the answers to these questions for the case of scalar-field boson stars (BSs), which are self-gravitating equilibrium solutions to the Einstein-Klein-Gordon equations [6–8].

*Contact author: te307@cam.ac.uk
†Contact author: U.Sperhake@damtp.cam.ac.uk
‡Contact author: ir346@cam.ac.uk
§Contact author: m.agathos@qmul.ac.uk

BSs have attracted a great deal of interest over the years. BSs may account for part of the enigmatic dark-matter content of the Universe [9,10]. BS solutions cover a wide range of compactness, thus forming a theoretical laboratory for exploring extreme-gravity effects beyond BHs such as the geometry of BS shadows [11,12] or light rings [13–15]. BSs are an ideal proxy for a wide class of compact binaries systematically deviating from BH systems, e.g., through finite tidal deformability [16]. Combined with their high amenability to numerical modeling, this makes BS binaries particularly suitable for high-precision gravitational-wave (GW) source modeling and template construction beyond BHs. Numerical studies of BS binaries have made tremendous progress in the last decade, focusing in particular on the merger remnants [17–22], and analytic approximations have been employed for performing PE of BS binary signals [23–25] (see also Refs. [26,27] for searches of Proca-star head-on collisions in GW data). Here, we numerically compute the first high-precision ∼20 orbit inspiral-merger-ringdown (IMR) waveforms for quasicircular BS binaries and inject them into LIGO detector noise. We perform PE using Bayesian inference and assess the ability of present BBH and binary NS waveform templates to recover the injected signals. We use natural units $c = 1 = \hbar$, i.e., $G = M_{\rm Pl}^{-2}$.

Theory—BSs in general relativity are described by the action of a complex scalar field φ minimally coupled to gravity,

$$S = \int \frac{\sqrt{-g}}{2}\left\{\frac{R}{8\pi G} - [g^{\mu\nu}\nabla_\mu\bar{\varphi}\nabla_\nu\varphi + V(\varphi)]\right\}\mathrm{d}^4x, \quad (1)$$

where $V(\varphi)$ is the potential, which we choose to be of solitonic type [28,29], $V_{\rm sol} = \mu^2|\varphi|^2(1-2|\varphi|^2/\sigma_0^2)^2$ with

$\sigma_0 = 0.2$. This choice allows us to construct BSs over a particularly wide range of compactness. Through appropriate re-scaling of the variables [30], the mass of the scalar can be set to $\mu = 1$ which, henceforth, sets the length scale of our units. Varying the action (1) yields the Einstein-Klein-Gordon equations and spherically symmetric solutions are obtained by decomposing the scalar field into amplitude A and frequency ω, $\varphi(t,r) = A(r)e^{i(\epsilon\omega t+\delta\phi)}$ [31]. Here we introduce the parameter $\epsilon = \pm 1$, determining the rotation of the scalar field in the complex plane, and a phase offset $\delta\phi$. Our primary BS always has $\epsilon = 1, \delta\phi = 0$ and we refer to configurations with secondary parameters $(\delta\phi = 0, \epsilon = 1)$, $(\delta\phi = (\pi/2), \epsilon = 1)$, $(\delta\phi = \pi, \epsilon = 1)$, $(\delta\phi = 0, \epsilon = -1)$ as *in-phase*, *dephased*, *antiphase,* and *anti-BS* binaries, respectively. Given the central amplitude $A_{\rm ctr} = A(0)$, we obtain a BS solution via a shooting algorithm described in Ref. [31]. In this work, we consider two models: a compact "A17" star with $\sqrt{G}A_{\rm ctr} = 0.17$, dimensionless tidal deformability $\Lambda \sim 10$ [16], and compactness $\mathcal{C} = 0.2$ containing 0.99 of its total mass m within a radius $r_{99} = 3.97$, and a less compact "A147" star with $\sqrt{G}A_{\rm ctr} = 0.147$, $\Lambda \sim 1000$, $\mathcal{C} = 0.1$, and $r_{99} = 4.48$. Tidal deformability characterizes the stars'tidal interaction—the higher Λ, the more susceptible the BS is to tidal deformations and corresponding changes in the GW phase.

NR simulations—Our simulations have been performed using two codes, GRChombo [32–34] and LEAN [35]. Both codes evolve the Einstein equations through fourth-order finite differencing of the CCZ4 formulation [36], employing the moving puncture gauge [37,38]. While GRChombo is based on adaptive-mesh refinement provided by CHOMBO [39], the LEAN code, based on the CACTUS computational toolkit [40], utilizes mesh refinement via CARPET [41]. Apparent horizons are computed using AHFINDERDIRECT [42]. We use a computational domain of length $L = 1024$ with bitant symmetry, 8 nested refinement levels with resolutions $\Delta x = 1/40$ to $1/48$ on the innermost level and extract GWs at $R_{\rm ex} \in [140, 240]$.

We focus on equal-mass nonspinning BS binaries of total mass $M = 2m$, listed in Table I, starting from initial data constructed as in Refs. [31,43]. By tuning the initial velocities, we reduce their orbital eccentricity, estimated according to Eq. (17) of Ref. [44], as 0.002–0.005. By verifying convergence of the A17 and A147 BS binaries and extrapolating GW signals to infinity, we obtain an error budget of $(0.1, 4\%)$ for the GW phase and amplitude for A17 binaries and $(0.2, 4\%)$ for A147 binaries, similar to finite differencing production runs for BH inspirals reported in Ref. [45]; see the Supplemental Material for details [46].

In physical terms, the most conspicuous difference between the A17 and A147 binary families of Table I is their ultimate fate. The compact A17 coalescences ubiquitously result in the formation of a BH remnant with dimensionless final spin $a_{\rm fin} \sim 0.7$, similar to the end product of nonspinning equal-mass BH mergers. By eye, the resulting GW form looks indistinguishable from a BH signal; cf. Fig. 1. In contrast, the "fluffy" A147 binaries merge into a more compact, highly distorted BS remnant with an oscillating central amplitude $0.156 \leq \sqrt{G}A_{\rm ctr} \leq 0.164$. The GW signal emitted by these fluffy binaries is characterized by a lower-amplitude inspiral part followed by an immense GW burst at merger and a prolonged, rapidly pulsating ringdown; cf. Fig. 1.

TABLE I. Summary of the BS binaries evolved in the center-of-mass frame with initial boost velocity $v_{x,\rm ini}$ in the x direction, impact parameter b in the y direction and separation d in the x direction. The dephased, antiphase, and anti-BS binaries are labeled as p090, p180, e1. $E_{l=2}$ is the GW energy contained in the $l = 2$ modes.

Simulation	$v_{x,\rm ini}$	b/M	d/M	$E_{l=2}/M$
A17-d12	0.1671	12.283	0.2243	0.0333
A17-d12-p180	0.1671	12.283	0.2243	0.0353
A17-d12-e1	0.1671	12.283	0.2243	0.0299
A17-d14	0.1533	14.017	0.2102	0.0346
A17-d15	0.14625	15.087	0.2033	0.0367
A17-d15-p090	0.14625	15.087	0.2033	0.0377
A17-d15-p180	0.14625	15.087	0.2033	0.0387
A17-d15-e1	0.14625	15.087	0.2033	0.0352
A147-d17	0.1389	16.639	0.0693	0.0589
A147-d19	0.1256	19.412	0.1109	0.0691

For the A17 family of stars we consider additional configurations with nonzero phase offsets, $\delta\phi = \pi/2, \pi$ and anti-BS binaries. All A17 binaries produce identical signals in the early inspiral, but as the BSs get closer, the scalar-field interaction [55,56] leads to delayed mergers for $\delta\phi \neq 0$, $\epsilon = -1$ and, especially, for $\delta\phi = \pi$. A comparison with BH waveforms [33] furthermore suggests that the A17 anti-BS signal resembles most closely that from a

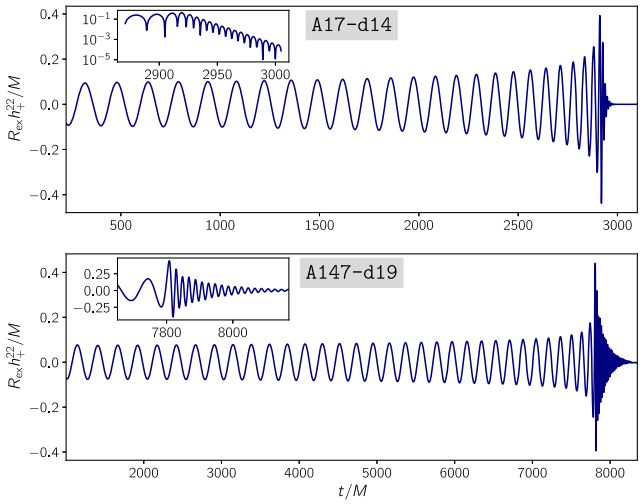

FIG. 1. Plus polarizations of the 22 IMR mode for the A17-d14 and A147-d19 binaries of Table I.

nonspinning, equal-mass BH binary in terms of the GW amplitude in the late inspiral and its phase evolution close to merger; cf. Fig. 3 in the Supplemental Material [46].

Parameter estimation—We inject our numerically computed GW signals into Gaussian noise colored by the O4 design sensitivities of the LIGO Hanford (H1) and Livingston (L1) detectors [2] and perform Bayesian inference using BILBY [57,58]. We focus on the dominant $l = 2$ modes and consider systems of total masses $M_{\rm tot}^{\rm inj} \in [5, 105] M_\odot$ in the source frame, corresponding to scalar-field masses $\mu \in [10^{-13}, 10^{-12}]$ eV. We choose luminosity distances $d_{\rm L}$ corresponding to (zero-noise) optimal injected signal-to-noise ratios (SNRs) $\rho^{\rm H1} \in [15, 60]$, $\rho^{\rm L1} \in [10, 45]$. We recover injected BS signals using standard waveform approximants, including effects of asymmetric mass ratio, spin, orbital precession and tides, as used routinely by the LIGO-Virgo-KAGRA Collaboration [3]: `IMRPhenomD` [59,60], `IMRPhenomPv3` [61], `IMRPhenomXP`, `IMRPhenomXPHM` [62], `TaylorF2` [63], `IMRPhenomPv2_NRTidal` [64,65] and `TEOBResumS` [66]. We obtain comparable results for the various approximants, as reviewed in more detail in the Supplemental Material [46], and focus the following discussion on `IMRPhenomXP` and `IMRPhenomPv2_NRTidal`. We report the mass values in the source frame; quantities in the detector frame will be denoted by "det"

We perform our inference using two sets of BBH-like spin priors: (i) we fix the spins in the recovery templates to their zero injected values; (ii) we explore the complete spin prior with all parameters being free. In the process, we compute for each detector the optimal SNR ρ of the recovered and injected signals. For each recovery we compute the Bayes factor $\mathcal{B}_{\rm N}^{\rm S}$, quantifying the evidence ratio between a signal being present in the data relative to the hypothesis of pure Gaussian noise. To assess the quality of the recovery we additionally compute the residual $r := d - h_{\rm max}$ from the data stream d and the approximant's strain $h_{\rm max}$ evaluated at the maximum-joint-log-likelihood source parameters across H1/L1. Specifically, we construct a null distribution of the white-noise optimal SNR for a signal duration D by generating random noise realizations via

$$n_{\rm w} := \frac{\tilde{n}(f)}{\sqrt{S_n(f)}} \sim \mathcal{N}\left(0, \frac{1}{2}\sqrt{D}\right), \tag{2}$$

where $S_n(f)$ is the detector's noise power-spectral density. If the residual's SNR falls above the 99th percentile of the noise SNR, we regard the residual as incompatible with Gaussian noise.

Results (`A17` families)—For the compact `A17` binaries, which form a BH postmerger, all waveform approximants enable confident recovery of the signals with a residual compatible with Gaussian noise, regardless of the analysis type; see Table II for a representative set of examples. Approximants including tidal effects furthermore infer tidal deformability parameters consistent with the injected $\Lambda_{1,2} \sim \mathcal{O}(10)$, albeit with poor constraints on Λ_2. This corresponds to a well measured tidal deformability $\delta\tilde{\Lambda}$ of the binary, but a poorly constrained $\tilde{\Lambda}$ [67]. All waveform approximants, however, fail to correctly infer some other injected parameters (component masses, spins and/or luminosity distance) within the 90% credible region; cf. Fig. 2 for a typical example. Provided the inspiral contributes significantly to the SNR, i.e., for $M_{\rm tot}^{\rm inj} \lesssim 80 M_\odot$

TABLE II. Recovery results for a range of BS injections from Table I using the `IMRPhenomXP` approximant with spins fixed to zero. We contrast the injected ($\rho_{\rm net}^{\rm inj}$) and recovered ($\rho_{\rm net}^{\rm rec}$) network SNRs and report the recovered chirp-masses $\mathcal{M}_{\rm c}^{\rm rec}$, mass-ratios $q^{\rm rec}$ at maximum-joint-log-likelihood.

Run	$\log \mathcal{B}_{\rm N}^{\rm S}$	$\rho_{\rm net}^{\rm inj}$	$\rho_{\rm net}^{\rm rec}$	$\mathcal{M}_{\rm c}^{\rm rec}/M_\odot$	$q^{\rm rec}$
$M_{\rm tot}^{\rm inj} = 72.4 M_\odot$, $\mathcal{M}_{\rm c}^{\rm inj} = 31.5 M_\odot$, $d_L^{\rm inj} = 500$ Mpc					
`A17-d12`	717	40.37	38.63	26.60	0.32
`A17-d15-p090`	1019	45.17	46.74	31.63	0.65
`A17-d12-p180`	792	43.84	36.62	25.07	0.97
`A17-d12-e1`	820	41.12	41.91	27.13	0.71
`A17-d14`	678	41.41	38.26	26.72	0.30
`A147-d19`	555	57.75	32.16	40.02	1.00
$M_{\rm tot}^{\rm inj} = 9.9 M_\odot$, $\mathcal{M}_{\rm c}^{\rm inj} = 4.3 M_\odot$, $d_L^{\rm inj} = 62.5$ Mpc					
`A17-d12`	406	29.69	30.60	3.89	0.39
`A17-d15-p090`	698	39.15	38.73	4.07	0.93
`A17-d12-p180`	328	30.91	28.28	3.94	1.00
`A17-d12-e1`	407	30.13	29.07	4.03	0.92
`A17-d14`	536	34.13	34.24	3.92	0.40
`A147-d19`	286	37.73	24.45	4.41	0.13

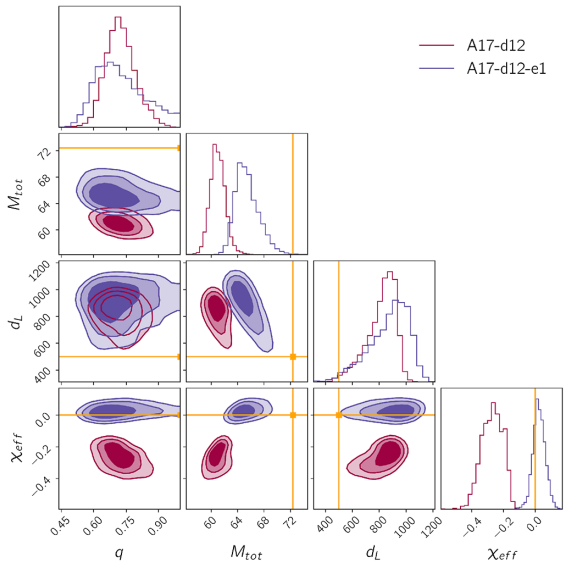

FIG. 2. Comparison of key PE results for `A17-d12` and `A17-d12-e1` injections. We use `IMRPhenomXP` for recovery of a BS binary with $M_{\rm tot}^{\rm inj} = 72.4 M_\odot$, $d_{\rm L} = 500$ Mpc and allow all binary parameters to be sampled over. The 1, 1.5, 2-sigma contours are shown.

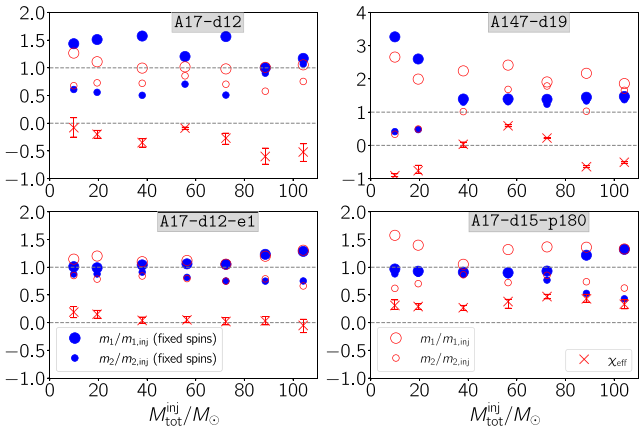

FIG. 3. PE results obtained for four BS families and injections with total mass $M^{\mathrm{inj}}_{\mathrm{tot}} \in [5, 105] M_\odot$ and luminosity distance $d_L = (M^{\mathrm{det}}_{\mathrm{tot}}/80M_\odot)500$ Mpc. For each injection, we display the median values of the recovered component masses m_1, m_2 normalized by their injected values (large and small circles) and the effective spin (crosses with 90% confidence interval). The recoveries are obtained for fixed (blue) or variable spins (red symbols). The dashed lines mark the injected values, 1 for the masses and 0 for χ_{eff}. The recovered parameters deviate from these values non-randomly; cf. the main text. By repeating selected injections with different d_{L}, we have verified that the displayed trends are robust under variations of the SNR.

in our case, however, these deviations are not random but exhibit clear systematics which we illustrate in Fig. 3 for a wide range of injections and now discuss in more detail.

`A17`, $\delta\phi = 0$, $\epsilon = 1$: We obtain consistent results for using either of the three waveform lengths employed, `d12`, `d14` and `d15`, indicating that they are sufficiently long for the mass range considered. In general, the recovered luminosity distance is overestimated, likely compensating for amplitude effects arising from biases in the other parameters. Next, the posteriors from BH approximants employed with spins fixed to zero systematically peak at total mass values within ∼10% of the injected $M^{\mathrm{inj}}_{\mathrm{tot}}$. For $M^{\mathrm{inj}}_{\mathrm{tot}} \lesssim 80M_\odot$, mass ratios are recovered with peaks in the range $0.3 \lesssim q := m_2/m_1 \lesssim 0.7$, with no posteriors supporting the injected $q = 1$ at 90% confidence. This picture changes considerably when we allow the spins to be sampled over in the prior. Then we obtain more accurate estimates for the primary mass m_1, often supporting the injected mass inside the 90% confidence interval, and larger mass ratios $0.5 \lesssim q \lesssim 0.85$, albeit still well below the injected $q = 1$. We furthermore infer significant spin magnitudes peaking at $0.3 \leq a_{1,2} \leq 0.98$ with clear preference for negatively aligned spins, i.e., $\chi_{\mathrm{eff}} < 0$.

`A17-p180`, $\delta\phi = \pi$, $\epsilon = 1$: As for $\delta\phi = 0$, the recovered luminosity distance is often overestimated. Quite remarkably, however, these antiphase binaries result in nearly opposite behaviour in PE results in every other regard. For $M^{\mathrm{inj}}_{\mathrm{tot}} \lesssim 80M_\odot$, we obtain good estimates for the primary mass m_1 and large mass ratios $q \geq 0.8$ when the spins are *fixed* to their injected values. Allowing the spins to vary, now results in significant overestimates of m_1 and more unequal mass ratios $0.3 \leq q \leq 0.8$. We typically obtain large spin magnitudes $a_{1,2} \geq 0.5$ but preferably exhibiting partial alignment with the orbital angular momentum, $0.1 \leq \chi_{\mathrm{eff}} \leq 0.5$.

`A17-d090`, $\delta\phi = \pi/2$, $\epsilon = 1$: This family of BS injections yields qualitatively similar behavior as `A17-p180`, but with generally smaller departure from the injected parameters.

`A17-e1`, $\delta\phi = 0$, $\epsilon = -1$: The anti-BS family is the best recovered of all our injections, supporting our conjecture that these binaries most closely resemble waveforms from nonspinning BHs. We typically obtain mass ratios $q \gtrsim 0.75$, where the primary mass m_1 is either contained inside the 90% confidence interval or close by, and, for $M^{\mathrm{inj}}_{\mathrm{tot}} \gtrsim 20M_\odot$, spin values close to zero. We illustrate this behavior by comparing in Fig. 2 a representative $M^{\mathrm{inj}}_{\mathrm{tot}} = 72.4M_\odot$ example of this family with its less accurately recovered `A17-d12` counterpart.

Interpretation: The most pronounced difference between $\delta\phi = 0$ BS binary signals, compared to their antiphase counterparts, is the steep increase of the GW amplitude in the late inspiral and merger whereas for $\delta\phi = \pi$, this *chirp* is shallower; cf. Fig. 3 in the Supplemental Material [46]. A closer inspection of GW signals from nonspinning BH binaries in the frequency domain similarly yields a steeper increase in the GW amplitude close to merger for unequal masses relative to $q = 1$. Unequal-mass BH chirps therefore resemble more closely those from $\delta\phi = 0$ BS binaries while $\delta\phi = \pi$ BS chirps are better approximated by equal-mass BH binaries.

The inclusion of spins allows for an additional adjustment of the chirp's steepness, typically boosting $\log(\mathcal{B}^{\mathrm{S}}_{\mathrm{N}})$ by ∼10%. BH binaries with aligned spins have an enhanced yet shallower inspiral than those with anti-aligned spins; see, e.g., Figs. 1 and 3 in [68]. The shallow inspiral-merger transition of $\delta\phi = \pi$ binaries, therefore, favors the "hang-up" of aligned spins whereas the more abrupt transition of $\delta\phi = 0$ BS binaries favors partially antialigned spins. This effect also sheds light on the mass-ratio drifts when we allow the spins to vary. For spins fixed at zero, the steep chirp of $\delta\phi = 0$ BS binaries can *only* be reproduced through an unequal mass ratio in the BBH approximant. For variable spins, in contrast, it can at least partly be accommodated through anti-aligned spins (the anti-hang-up effect); statistically we then expect a drift towards $q = 1$. For $\delta\phi = \pi$ BS binaries, in turn, the inclusion of spins enables BILBY to reproduce the shallow chirp in the BS signal through aligned spins rather than resorting *exclusively* to a high ($q \approx 1$) mass ratio; this results in a drift towards smaller q.

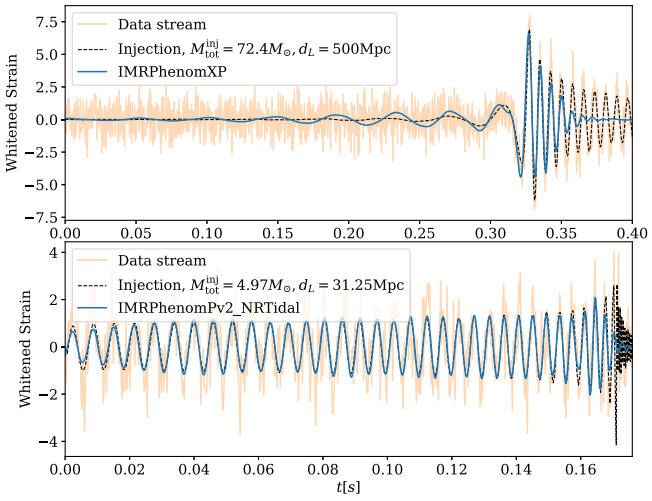

FIG. 4. *Top:* The recovery of a high-mass `A147-d19` binary injection using `IMRPhenomXP` results in $m_1 \sim 70 M_\odot$, $m_2 \sim 65 M_\odot$, $a_1 \sim 0.98$, and $a_2 \sim 0.60$. *Bottom:* The recovery of a low-mass `A147-d19` binary injection using `IMRPhenomPv2_NRTidal` yields maximum-joint-log-likelihood estimates $m_1 \sim 3.7 M_\odot$, $m_2 \sim 1.3 M_\odot$, $a_1 \sim 0.96$, $a_2 \sim 0.63$, $\Lambda_1 \sim 3000$, and $\Lambda_2 \sim 11000$.

Results (`A147` family)—As illustrated in Fig. 1, GW signals from our less compact `A147` family of BS binaries differ more pronouncedly from BH waveforms, especially around merger and ringdown. These differences manifest themselves not only in the form of PE biases, but also an incomplete recovery of the injected signals. In particular, for high (low) total mass $M_{\rm tot}^{\rm inj}$, the approximants are able to match the merger (inspiral) part of the signals but never both and never the ringdown; cf. Fig. 4. Overall, this leads to a reduction in the recovered optimal SNR compared to the injection; cf. Table II. For injections with $\rho_{\rm inj} \lesssim 30$, the residual is still consistent with noise but for $\rho_{\rm inj} \gtrsim 30$ we often obtain significant residuals.

Furthermore, the late inspiral of less compact BS binaries occurs at lower frequencies than that of compact ones, so that BBH approximants systematically overestimate the total mass; cf. Fig. 3. The addition of tidal effects improves the approximant's ability to capture features in the inspiral portion of the signal for small $M_{\rm tot}^{\rm inj}$; we thus obtain large tidal parameters $\Lambda_{1,2} \sim 10^3$ to 10^4 consistent with the BS binary, albeit with large uncertainties in Λ_2. Similar to the compact BS injections, overall the inclusion of tidal effects does not improve the estimation of other injection parameters.

Conclusions—By performing high-precision NR simulations of inspiralling and merging BS binaries, we have investigated the capability of current waveform models to recover BS GW signals with the following key results. (i) Most BS systems considered here are detectable with current GW analysis pipelines although current waveform templates systematically infer incorrect source parameters. (ii) BS binaries can be numerically modeled with accuracy comparable to BH binaries. (iii) BSs are excellent candidate sources for constructing GW template banks alternative to BHs and NSs.

Our study suggests that, from the viewpoint of current GW detectors, BS signals exhibit significant degeneracy with BBH waveforms obstructing the distinction between BS binaries, especially those forming a BH upon merger, and NS or BH systems. The most notable exception from this degeneracy consists in the exceptionally strong inspiral-merger transition and a long-lived ringdown in binaries forming a BS postmerger; both these features are generally poorly matched by present approximants leaving behind non-Gaussian residuals.

Acknowledgments—We thank Priscilla Canizares and Christopher J. Moore for fruitful discussions on GW analysis and the GRTL collaboration [69]. T. E. is supported by the Centre for Doctoral Training at the University of Cambridge funded through STFC. I. M. R.-S. acknowledges support from the Herchel Smith Postdoctoral Fellowship Fund. This work has been supported by STFC Research Grant No. ST/V005669/1. We acknowledge support by the NSF Grants No. PHY-090003, No. PHY-1626190, and No. PHY-2110594, DiRAC projects ACTP284 and ACTP238, STFC capital Grants No. ST/P002307/1, No. ST/R002452/1, No. ST/I006285/1, and No. ST/V005618/1, STFC operations Grant No. ST/R00689X/1. Computations were done on the CSD3 and Fawcett (Cambridge), Cosma (Durham), Hawk (Cardiff), CIT LIGO Lab (Pasadena), Stampede2 (TACC), and Expanse (SDSC) clusters.

Data availability—Our data and animations are publicly available [70–72].

[1] B. P. Abbott *et al.*, Observation of gravitational waves from a binary black hole merger, Phys. Rev. Lett. **116**, 061102 (2016).
[2] B. P. Abbott *et al.* (KAGRA, LIGO Scientific, and Virgo Collaborations), Prospects for observing and localizing gravitational-wave transients with Advanced LIGO, Advanced Virgo and KAGRA, Living Rev. Relativity **21**, 3 (2018).
[3] R. Abbott *et al.* (KAGRA, Virgo, and LIGO Scientific Collaborations), GWTC-3: Compact binary coalescences observed by LIGO and Virgo during the second part of the third observing run, Phys. Rev. X **13**, 041039 (2023).
[4] A. H. Nitz, S. Kumar, Y.-F. Wang, S. Kastha, S. Wu, M. Schäfer, R. Dhurkunde, and C. D. Capano, 4-OGC: Catalog of gravitational waves from compact binary mergers, Astrophys. J. **946**, 59 (2023).
[5] V. Cardoso and P. Pani, Testing the nature of dark compact objects: A status report, Living Rev. Relativity **22**, 4 (2019).

[6] D. J. Kaup, Klein-Gordon Geon, Phys. Rev. **172**, 1331 (1968).

[7] R. Ruffini and S. Bonazzola, Systems of self-gravitating particles in general relativity and the concept of an equation of state, Phys. Rev. **187**, 1767 (1969).

[8] S. L. Liebling and C. Palenzuela, Dynamical boson stars, Living Rev. Relativity **26**, 1 (2023).

[9] R. Sharma, S. Karmakar, and S. Mukherjee, Boson star and dark matter, arXiv:0812.3470.

[10] D. J. E. Marsh, Axion cosmology, Phys. Rep. **643**, 1 (2016).

[11] F. H. Vincent, Z. Meliani, P. Grandclement, E. Gourgoulhon, and O. Straub, Imaging a boson star at the Galactic center, Classical Quantum Gravity **33**, 105015 (2016).

[12] J. L. Rosa and D. Rubiera-Garcia, Shadows of boson and Proca stars with thin accretion disks, Phys. Rev. D **106**, 084004 (2022).

[13] P. Grandclément, Light rings and light points of boson stars, Phys. Rev. D **95**, 084011 (2017).

[14] P. V. P. Cunha, E. Berti, and C. A. R. Herdeiro, Light-ring stability for ultracompact objects, Phys. Rev. Lett. **119**, 251102 (2017).

[15] P. V. P. Cunha, C. Herdeiro, E. Radu, and N. Sanchis-Gual, Exotic compact objects and the fate of the light-ring instability, Phys. Rev. Lett. **130**, 061401 (2023).

[16] N. Sennett, T. Hinderer, J. Steinhoff, A. Buonanno, and S. Ossokine, Distinguishing boson stars from black holes and neutron stars from tidal interactions in inspiraling binary systems, Phys. Rev. D **96**, 024002 (2017).

[17] C. Palenzuela, P. Pani, M. Bezares, V. Cardoso, L. Lehner, and S. Liebling, Gravitational wave signatures of highly compact boson star binaries, Phys. Rev. D **96**, 104058 (2017).

[18] M. Bezares, M. Bošković, S. Liebling, C. Palenzuela, P. Pani, and E. Barausse, Gravitational waves and kicks from the merger of unequal mass, highly compact boson stars, Phys. Rev. D **105**, 064067 (2022).

[19] R. Croft, T. Helfer, B.-X. Ge, M. Radia, T. Evstafyeva, E. A. Lim, U. Sperhake, and K. Clough, The gravitational afterglow of boson stars, Classical Quantum Gravity **40**, 065001 (2023).

[20] N. Siemonsen and W. E. East, Generic initial data for binary boson stars, Phys. Rev. D **108**, 124015 (2023).

[21] N. Siemonsen and W. E. East, Binary boson stars: Merger dynamics and formation of rotating remnant stars, Phys. Rev. D **107**, 124018 (2023).

[22] N. Siemonsen, Nonlinear treatment of a black hole mimicker ringdown, Phys. Rev. Lett. **133**, 031401 (2024).

[23] C. Pacilio, M. Vaglio, A. Maselli, and P. Pani, Gravitational-wave detectors as particle-physics laboratories: Constraining scalar interactions with a coherent inspiral model of boson-star binaries, Phys. Rev. D **102**, 083002 (2020).

[24] M. Vaglio, C. Pacilio, A. Maselli, and P. Pani, Bayesian parameter estimation on boson-star binary signals with a coherent inspiral template and spin-dependent quadrupolar corrections, Phys. Rev. D **108**, 023021 (2023).

[25] H.-K. Guo, K. Sinha, and C. Sun, Probing boson stars with extreme mass ratio inspirals, J. Cosmol. Astropart. Phys. 09 (2019) 032.

[26] J. C. Bustillo, N. Sanchis-Gual, A. Torres-Forné, J. A. Font, A. Vajpeyi, R. Smith, C. Herdeiro, E. Radu, and S. H. W. Leong, GW190521 as a merger of Proca stars: A potential new vector boson of 8.7×10^{-13} eV, Phys. Rev. Lett. **126**, 081101 (2021).

[27] J. Calderon Bustillo, N. Sanchis-Gual, S. H. W. Leong, K. Chandra, A. Torres-Forne, J. A. Font, C. Herdeiro, E. Radu, I. C. F. Wong, and T. G. F. Li, Searching for vector boson-star mergers within LIGO-Virgo intermediate-mass black-hole merger candidates, Phys. Rev. D **108**, 123020 (2023).

[28] T. D. Lee and Y. Pang, Nontopological solitons, Phys. Rep. **221**, 251 (1992).

[29] T. D. Lee, Soliton stars and the critical masses of black holes, Phys. Rev. D **35**, 3637 (1987).

[30] T. Evstafyeva, R. Rosca-Mead, U. Sperhake, and B. Brugmann, Boson stars in massless and massive scalar-tensor gravity, Phys. Rev. D **108**, 104064 (2023).

[31] T. Helfer, U. Sperhake, R. Croft, M. Radia, B.-X. Ge, and E. A. Lim, Malaise and remedy of binary boson-star initial data, Classical Quantum Gravity **39**, 074001 (2022).

[32] K. Clough, P. Figueras, H. Finkel, M. Kunesch, E. A. Lim, and S. Tunyasuvunakool, GRChombo: Numerical relativity with adaptive mesh refinement, Classical Quantum Gravity **32**, 245011 (2015).

[33] M. Radia, U. Sperhake, A. Drew, K. Clough, P. Figueras, E. A. Lim, J. L. Ripley, J. C. Aurrekoetxea, T. França, and T. Helfer, Lessons for adaptive mesh refinement in numerical relativity, Classical Quantum Gravity **39**, 135006 (2022).

[34] T. Andrade *et al.*, GRChombo: An adaptable numerical relativity code for fundamental physics, J. Open Source Software **6**, 3703 (2021).

[35] U. Sperhake, Binary black-hole evolutions of excision and puncture data, Phys. Rev. D **76**, 104015 (2007).

[36] D. Alic, C. Bona-Casas, C. Bona, L. Rezzolla, and C. Palenzuela, Conformal and covariant formulation of the Z4 system with constraint-violation damping, Phys. Rev. D **85**, 064040 (2012).

[37] M. Campanelli, C. O. Lousto, P. Marronetti, and Y. Zlochower, Accurate evolutions of orbiting black-hole binaries without excision, Phys. Rev. Lett. **96**, 111101 (2006).

[38] J. G. Baker, J. Centrella, D.-I. Choi, M. Koppitz, and J. van Meter, Gravitational wave extraction from an inspiraling configuration of merging black holes, Phys. Rev. Lett. **96**, 111102 (2006).

[39] M. Adams *et al.*, Chombo Software Package for AMR applications—design document, Technical Report LBNL-6616E, Lawrence Berkeley National Laboratory, 2019.

[40] G. Allen, T. Goodale, J. Massó, and E. Seidel, The Cactus computational toolkit and using distributed computing to collide neutron stars, in *Proceedings of Eighth IEEE International Symposium on High Performance Distributed Computing, HPDC-8, Redondo Beach, 1999* (IEEE Press, Piscataway, New Jersey, United States, 1999).

[41] E. Schnetter, S. H. Hawley, and I. Hawke, Evolutions in 3-D numerical relativity using fixed mesh refinement, Classical Quantum Gravity **21**, 1465 (2004).

[42] J. Thornburg, A fast apparent horizon finder for three-dimensional Cartesian grids in numerical relativity, Classical Quantum Gravity **21**, 743 (2004).

[43] T. Evstafyeva, U. Sperhake, T. Helfer, R. Croft, M. Radia, B.-X. Ge, and E. A. Lim, Unequal-mass boson-star binaries: initial data and merger dynamics, Classical Quantum Gravity **40**, 085009 (2023).
[44] A. H. Mroue, H. P. Pfeiffer, L. E. Kidder, and S. A. Teukolsky, Measuring orbital eccentricity and periastron advance in quasi-circular black hole simulations, Phys. Rev. D **82**, 124016 (2010).
[45] I. Hinder *et al.*, Error-analysis and comparison to analytical models of numerical waveforms produced by the NRAR Collaboration, Classical Quantum Gravity **31**, 025012 (2014).
[46] See Supplemental Material at http://link.aps.org/supplemental/10.1103/PhysRevLett.133.131401, which includes Refs. [47–54], for convergence tests and details of our injections.
[47] LIGO Scientific, Virgo, and KAGRA Collaborations, LVK Algorithm Library—LALSuite, Free software (GPL) (2018).
[48] K. Wette, SWIGLAL: PYTHON and Octave interfaces to the LALSuite gravitational-wave data analysis libraries, SoftwareX **12**, 100634 (2020).
[49] P. Schmidt, I. W. Harry, and H. P. Pfeiffer, Numerical relativity injection infrastructure, arXiv:1703.01076.
[50] J. S. Speagle, DYNESTY: A dynamic nested sampling package for estimating Bayesian posteriors and evidences, Mon. Not. R. Astron. Soc. **493**, 3132 (2020).
[51] W. Del Pozzo and J. Veitch, CPNest: Parallel nested sampling, Astrophysics Source Code Library, record ascl:2205.021 (2022).
[52] M. J. Williams, J.Veitch, C.Chapman-Bird, and R.Tenerio, nessai: Nested sampling with artificial intelligence (2021), 10.5281/zenodo.4550693.
[53] M. J. Williams, J. Veitch, and C. Messenger, Nested sampling with normalizing flows for gravitational-wave inference, Phys. Rev. D **103**, 103006 (2021).
[54] M. J. Williams, J. Veitch, and C. Messenger, Importance nested sampling with normalising flows, Mach. Learn. Sci. Tech. **4**, 035011 (2023).
[55] C. Palenzuela, I. Olabarrieta, L. Lehner, and S. L. Liebling, Head-on collisions of boson stars, Phys. Rev. D **75**, 064005 (2007).
[56] N. Sanchis-Gual, J. C. Bustillo, C. Herdeiro, E. Radu, J. A. Font, S. H. W. Leong, and A. Torres-Forné, Impact of the wavelike nature of Proca stars on their gravitational-wave emission, Phys. Rev. D **106**, 124011 (2022).
[57] G. Ashton *et al.*, BILBY: A user-friendly Bayesian inference library for gravitational-wave astronomy, Astrophys. J. Suppl. Ser. **241**, 27 (2019).
[58] I. M. Romero-Shaw *et al.*, Bayesian inference for compact binary coalescences with bilby: Validation and application to the first LIGO-Virgo gravitational-wave transient catalogue, Mon. Not. R. Astron. Soc. **499**, 3295 (2020).
[59] S. Husa, S. Khan, M. Hannam, M. Pürrer, F. Ohme, X. J. Forteza, and A. Bohé, Frequency-domain gravitational waves from nonprecessing black-hole binaries. I. New numerical waveforms and anatomy of the signal, Phys. Rev. D **93**, 044006 (2016).
[60] S. Khan, S. Husa, M. Hannam, F. Ohme, M. Pürrer, X. J. Forteza, and A. Bohé, Frequency-domain gravitational waves from nonprecessing black-hole binaries. II. A phenomenological model for the advanced detector era, Phys. Rev. D **93**, 044007 (2016).
[61] S. Khan, K. Chatziioannou, M. Hannam, and F. Ohme, Phenomenological model for the gravitational-wave signal from precessing binary black holes with two-spin effects, Phys. Rev. D **100**, 024059 (2019).
[62] G. Pratten *et al.*, Computationally efficient models for the dominant and subdominant harmonic modes of precessing binary black holes, Phys. Rev. D **103**, 104056 (2021).
[63] F. Messina and A. Nagar, Parametrized-4.5PN TaylorF2 approximants and tail effects to quartic nonlinear order from the effective one body formalism, Phys. Rev. D **95**, 124001 (2017); Phys. Rev. D **96**, 049907(E) (2017).
[64] T. Dietrich, S. Bernuzzi, and W. Tichy, Closed-form tidal approximants for binary neutron star gravitational waveforms constructed from high-resolution numerical relativity simulations, Phys. Rev. D **96**, 121501(R) (2017).
[65] T. Dietrich, A. Samajdar, S. Khan, N. K. Johnson-McDaniel, R. Dudi, and W. Tichy, Improving the NRTidal model for binary neutron star systems, Phys. Rev. D **100**, 044003 (2019).
[66] A. Nagar *et al.*, Time-domain effective-one-body gravitational waveforms for coalescing compact binaries with nonprecessing spins, tides and self-spin effects, Phys. Rev. D **98**, 104052 (2018).
[67] L. Wade, J. D. E. Creighton, E. Ochsner, B. D. Lackey, B. F. Farr, T. B. Littenberg, and V. Raymond, Systematic and statistical errors in a Bayesian approach to the estimation of the neutron-star equation of state using advanced gravitational wave detectors, Phys. Rev. D **89**, 103012 (2014).
[68] M. Campanelli, C. O. Lousto, and Y. Zlochower, Spinning-black-hole binaries: The orbital hang up, Phys. Rev. D **74**, 041501(R) (2006).
[69] https://github.com/GRTLCollaboration.
[70] T. Evstafyeva and U. Sperhake, Boson star waveforms (2024), https://github.com/tamaraevst/Boson-star-waveforms.
[71] T. Evstafyeva, U. Sperhake, I. Romero-Shaw, and M. Agathos, Inspiral and merger of equal-mass boson star binary forming a black hole post-merger (2024), https://www.youtube.com/watch?v=QrbJKKAOerY.
[72] T. Evstafyeva, U. Sperhake, I. Romero-Shaw, and M. Agathos, Inspiral and merger of equal-mass boson star binary forming a boson star post-merger (2024), https://www.youtube.com/watch?v=hj1WzNPpeS0.